

1 **Technical Note: Silica stable isotopes and silicification in a carnivorous sponge**

2 ***Asbestopluma* sp.**

3 Katharine R Hendry<sup>1</sup>, George EA Swann<sup>2</sup>, Melanie J Leng<sup>3,4</sup>, Hilary J Sloane<sup>3</sup>, Claire Goodwin<sup>5</sup>, Jade  
4 Berman<sup>6</sup>, and Manuel Maldonado<sup>7</sup>

5 <sup>1</sup> *School of Earth Sciences, University of Bristol, Wills Memorial Building, Queen's Road, Bristol, BS8*  
6 *1RJ, UK*

7 <sup>2</sup> *School of Geography, University of Nottingham, University Park, Nottingham, NG7 2RD, UK*

8 <sup>3</sup> *NERC Isotope Geosciences Facilities, British Geological Survey, Keyworth, Nottingham, NG12 5GG,*  
9 *UK*

10 <sup>4</sup> *Centre for Environmental Geochemistry, University of Nottingham, University Park, Nottingham,*  
11 *NG7 2RD, UK*

12 <sup>5</sup> *National Museums Northern Ireland, 153 Bangor Road, Cultra, Holywood, Co. Down, BT18 0EU, UK*

13 <sup>6</sup> *Ulster Wildlife, 3 New Line, Crossgar, Co Down, Northern Ireland, BT30 9EP, UK*

14 <sup>7</sup> *Centro de Estudios Avanzados de Blanes (CEAB-CSIC), Accés a la Cala St. Francesc, 14, Blanes 17300,*  
15 *Girona, Spain*

16

17 **Response to reviewer:**

18 Many thanks to the reviewer for their thoughtful reviews, and the time and effort spent to help us  
19 improve our manuscript.

20 **L261 : Authors should separate silicon and oxygen systems: variations in silicon and oxygen**  
21 **isotope fractionations**

22 We have specified this as requested.

23

24 **L354-359 : The claim that « heating samples of opal to over 70°C during cleaning does not result in**  
25 **additional fractionation of oxygen isotopes » should be nuanced. Crespin et al., (2010) previously**  
26 **showed that fractionation may happen at temperature higher than 70°C. The fact that « heating at**  
27 **higher temperatures is routine in downcore spicule opal  $\delta^{18}\text{O}$  analyses (e.g. Snelling et al., 2014) »**  
28 **is not a demonstration in itself. Was there any study demonstrating the absence of fractionation**  
29 **at 80°C ? Authors should be cautious about that matter.**

30 We have added the reference as required. We have changed the end of the paragraph to read:  
31 “Although there is no available information specifically about modern sponge spicules, heating  
32 samples of phytolith opal to 80°C during cleaning does not result in additional fractionation of  
33 oxygen isotopes (Crespin et al., 2008). One study suggests that heating diatom opal to over 60°C  
34 results in a potential offset in  $\delta^{18}\text{O}$  as a result of dissolution (Crespin et al., 2008). However, the  $\delta^{18}\text{O}$   
35 values from 70 and 90°C from this study were within analytical error of the values of diatoms treated  
36 at 60°C. Furthermore, heating of diatom opal to 70°C using different cleaning methods does not

37 result in measurable changes in  $\delta^{18}\text{O}$  (Tyler et al., 2007). Heating to higher temperatures of 80-90°C  
38 is routine in downcore spicule opal  $\delta^{18}\text{O}$  analyses (e.g. Snelling et al., 2014).”

39

40 **L420-422 : The sentence is not clear.**

41 We have restructured this sentence, and hope it is now clarified.

42

43 **L520-522 : This sentence is confusing. Although there might be no investigation of dissolution**  
44 **effect on  $\delta^{18}\text{O}$  value of sponge spicules themselves, it is reasonable to expect kinetic fractionation**  
45 **of oxygen (increase of  $\delta^{18}\text{O}$ ) due to dissolution of silicates. See Brandriss et al. (1998 ; GCA),**  
46 **Schmidt et al. (2001 ; GCA), Crespín et al. (2008, Anal. Chem) and Dodd et al. (2012, G3) for**  
47 **discussions on precipitation and dissolution processes affecting  $\delta^{18}\text{O}$  values of biogenic silica.**  
48 **Once more, authors should be more cautious about that matter.**

49 We have added two of the more recent papers to the discussion as requested. The end of the  
50 paragraph now reads: “Although there is potential for kinetic fractionation of oxygen during  
51 dissolution and reprecipitation of silica (Crespín et al., 2008; Dodd et al., 2012), further work is  
52 required to investigate whether fractionation of either silicon or oxygen isotopes occurs during the  
53 dissolution of sponge spicules, or by any additional surface precipitation processes

54

55 **Technical Note: Silica stable isotopes and silicification in a carnivorous sponge**

56 ***Asbestopluma* sp.**

57 Katharine R Hendry<sup>1</sup>, George EA Swann<sup>2</sup>, Melanie J Leng<sup>3,4</sup>, Hilary J Sloane<sup>3</sup>, Claire Goodwin<sup>5</sup>, Jade  
58 Berman<sup>6</sup>, and Manuel Maldonado<sup>7</sup>

59 <sup>1</sup> *School of Earth Sciences, University of Bristol, Wills Memorial Building, Queen's Road, Bristol, BS8*  
60 *1RJ, UK*

61 <sup>2</sup> *School of Geography, University of Nottingham, University Park, Nottingham, NG7 2RD, UK*

62 <sup>3</sup> *NERC Isotope Geosciences Facilities, British Geological Survey, Keyworth, Nottingham, NG12 5GG,*  
63 *UK*

64 <sup>4</sup> *Centre for Environmental Geochemistry, University of Nottingham, University Park, Nottingham,*  
65 *NG7 2RD, UK*

66 <sup>5</sup> *National Museums Northern Ireland, 153 Bangor Road, Cultra, Holywood, Co. Down, BT18 0EU, UK*

67 <sup>6</sup> *Ulster Wildlife, 3 New Line, Crossgar, Co Down, Northern Ireland, BT30 9EP, UK*

68 <sup>7</sup> *Centro de Estudios Avanzados de Blanes (CEAB-CSIC), Accés a la Cala St. Francesc, 14, Blanes 17300,*  
69 *Girona, Spain*

70

71 **Keywords:**

72 Silicon isotopes, oxygen isotopes, siliceous spicule, proxy

73 **Abstract:**

74           The stable isotope composition of benthic sponge spicule silica is a potential source of  
75 palaeoceanographic information about past deep seawater chemistry. The silicon isotope  
76 composition of spicules has been shown to relate to the silicic acid concentration of ambient  
77 water, although existing calibrations do exhibit a degree of scatter in the relationship. Less is  
78 known about how the oxygen isotope composition of sponge spicule silica relates to  
79 environmental conditions during growth. Here, we investigate the vital effects on silica silicon and  
80 oxygen isotope composition in a carnivorous sponge, *Asbestopluma* sp., from the Southern Ocean.  
81 We find significant variations in silicon and oxygen isotopic composition within the specimen that  
82 are related to unusual spicule silicification. The largest variation in both isotope systems was  
83 associated to the differential distribution of an unconventional, hypersilicified spicule type  
84 (desma) along the sponge body. The absence an internal canal in the desmas suggests an  
85 unconventional silicification pattern leading to an unusually heavy isotope signature. Additional  
86 internal variability derives from a systematic offset between the peripheral skeleton of the body  
87 having systematically a higher isotopic composition than the internal skeleton. A simplified silicon  
88 isotope fractionation model, in which desmas were excluded, suggests that the lack of a system  
89 for seawater pumping in carnivorous sponges favours a low replenishment of dissolved silicon  
90 within the internal tissues, causing kinetic fractionation during silicification that impacts the  
91 isotope signature of the internal skeleton. Analysis of multiple spicules should be carried out to  
92 “average out” any artefacts in order to produce more robust downcore measurements.

93 **Introduction:**

94 The formation of amorphous biogenic silica (or opal) by photosynthetic diatoms, which play a  
 95 major role in the export of organic matter to the seafloor, is a key part to both the cycling of silicon  
 96 and carbon in the Earth's climate system (Tréguer and De La Rocha, 2013). Quantifying the dissolved  
 97 silicon, or silicic acid ( $\text{Si}(\text{OH})_4$ ), concentration of upwelling waters is essential if we are to understand  
 98 the distribution and growth of diatoms in surface waters and so the drawdown on atmospheric carbon  
 99 dioxide (Hendry and Brzezinski, 2014). The silicon isotope ( $\delta^{30}\text{Si}$ ) and oxygen isotope ( $\delta^{18}\text{O}$ )  
 100 compositions of biogenic silica have been used to infer modern nutrient cycling, past nutrient supply  
 101 and utilization, and hydrological cycling. Whilst the isotope composition of diatom opal has been used  
 102 widely to understand past surface conditions (Leng et al., 2009), the chemical composition of benthic  
 103 dwelling, deep-sea sponge opal holds the potential to reveal insights into bottom water conditions.

104 Both silicon and oxygen are present in three stable isotopes:  $^{28}\text{Si}$  (92.22%),  $^{29}\text{Si}$  (4.68%) and  
 105  $^{30}\text{Si}$  (3.08%); and  $^{16}\text{O}$  (~99.7%),  $^{17}\text{O}$  (~0.04%) and  $^{18}\text{O}$  (~0.2%) respectively  
 106 (<http://www.nndc.bnl.gov/chart/>). The per mille Si isotopic composition is expressed relative to the  
 107 NIST standard, NBS 28, according to Equation 1, and similarly the O isotopic composition is expressed  
 108 relative to VSMOW, according to Equation 2:

109

$$110 \quad \delta^{30}\text{Si} = \left\{ \left[ \frac{\left( \frac{^{30}\text{Si}}{^{28}\text{Si}} \right)_{\text{sample}}}{\left( \frac{^{30}\text{Si}}{^{28}\text{Si}} \right)_{\text{NBS28}}} \right] - 1 \right\} \times 1000 \quad (1)$$

$$111 \quad \delta^{18}\text{O} = \left\{ \left[ \frac{\left( \frac{^{18}\text{O}}{^{16}\text{O}} \right)_{\text{sample}}}{\left( \frac{^{18}\text{O}}{^{16}\text{O}} \right)_{\text{VSMOW}}} \right] - 1 \right\} \times 1000 \quad (2)$$

112 Recent work has shown that  $\delta^{30}\text{Si}$  of a wide range of deep-sea sponges from different ocean  
 113 basins reflects the availability of dissolved silicon (silicic acid [ $\text{Si}(\text{OH})_4$ ]) during growth, with minimal  
 114 impact from temperature, pH and (to date, and on few studies) no systematic species-dependent  
 115 fractionation (Hendry and Robinson, 2012; Wille et al., 2010). With sponge spicules ubiquitous in  
 116 sediments throughout the ocean and with degradation occurring at rates that are an orders of  
 117 magnitude slower than those for diatoms and other siliceous organisms (Maldonado et al. 2005,  
 118 Maldonado et al. 2012), there is significant potential for spicules to be used as a proxy for past ocean  
 119 conditions. Whilst a number of papers have explored the use of  $\delta^{30}\text{Si}$  in sponges (e.g. Ellwood et al.,  
 120 2010; Hendry et al., 2014), there is still scatter in the calibration of the  $\delta^{30}\text{Si}$ - $\text{Si}(\text{OH})_4$  relationship,

121 with the sources of variability poorly understood. Likewise, little is known about the sponge spicule  
122 silica  $\delta^{18}\text{O}$ , although it is likely impacted by biological factors (Matteuzzo et al., 2013) that cause  
123 systematic offsets when compared to diatom silica  $\delta^{18}\text{O}$  (Snelling et al. 2014). Here, we investigate  
124 the impact of derived biomineralisation mechanisms that could be responsible for variations in  
125 [silicon and oxygen](#) isotope fractionation in sponges using a carnivorous sponge specimen from the  
126 Southern Ocean as a case study.

127

### 128 **Sponges and sponge biomineralisation:**

129 Sponges (Porifera) are sessile filter-feeding animals. Their body plan has evolutionarily been  
130 shaped to optimize the feeding function, evolving an architectural design that, in general, is shared  
131 by the four major sponge lineages (Demospongiae, Hexactinellida, Homosclerophorida, and  
132 Calcareaea). The anatomical archetype of a sponge is a vase-shaped or oblate body crossed by a  
133 system of aquiferous canals that communicate to the outside at both ends, and through which a  
134 current of environmental water flows, transporting bacteria and dissolved compounds that nourish  
135 the sponge, oxygen and waste products. The histological archetype of a sponge consists of two  
136 epithelial layers of flattened cells (pinacocytes), an external layer that forms the wall of the body,  
137 and an internal layer that forms the wall of the aquiferous canals. Between the epithelium of the  
138 canals and the external epithelium, there is a mesenchyme-like zone that is rich in collagen and is  
139 populated by different groups of mobile amoeboid cells. The spicules (i.e., siliceous or calcareous  
140 skeletal pieces that give structural support to these often soft-bodied organisms) are also produced  
141 and assembled together by cells (i.e. sclerocytes) in the mesenchyme-like zone. The aquiferous  
142 canals include chamber-shaped expansions, in which the walls are coated not by pinacocytes but  
143 choanocytes that is pseudocylindrical cells possessing a flagellum surrounded by a collar of microvilli  
144 at the distal pole. These cells phagocytose picoplankton from the water passing through the  
145 chambers; they are the most distinctive feature of the phylum Porifera.

146 However, a group of demosponges, currently mainly classed in the family Cladorhizidae  
147 (Order Poecilosclerida), have evolved a carnivorous habit (Vacelet, 2006), thought to be an  
148 adaptation to the nutrient-poor environments in which they inhabit, where a 'sit-and-wait'  
149 predatory strategy is beneficial because of the low energy expenditure between rare feeding  
150 opportunities (Vacelet and Duport, 2004; Vacelet, 2007). Carnivorous sponges are usually associated  
151 with low nutrient mid basin areas of the deep-sea (the deepest recorded at 8840m) but a few are  
152 found around 100m depth in high latitudes and some species have also been found in shallow  
153 sublittoral and littoral caves in the Mediterranean, where they are thought to have colonised from  
154 deep-water populations (Aguilar et al., 2011; Bakran-Petricioli et al., 2007; Chevaldonné et al., 2014;

155 Lopes, et al., 2012; Vacelet, 2006, 2007). These carnivorous sponges show not only an unusual  
156 internal body organization lacking choanocytes and aquiferous canals, but also a convergence  
157 towards characteristic morphological adaptations including an upright stalked body, with branches,  
158 and feather-like or balloon-like lateral expansions to enhance encounter rates with prey.  
159 Carnivorous sponges have developed either rhizoid-like or bulbous bases for holding their erect  
160 bodies on muddy and hard substrates respectively (Vacelet, 2007).

161           The family Cladorhizidae, despite being relatively small (7 genera, 140 spp.; Porifera World  
162 Database, September 2014), has a moderate diversity of spicules. In these sponges, the silica  
163 spicules are needed not only to provide skeletal support to the body, but also to capture prey. Their  
164 relatively small bodies (rarely taller than 10 cm) usually have an internal, central skeletal core (axial  
165 skeleton) made by a bundle of highly-packed needle-like spicules, typically shorter than 700  $\mu\text{m}$   
166 each, and with one or both ends being pointed (i.e., monactinal or diactinal megascleres). From this  
167 axial skeleton radiating spicule tracts diverge (extra-axial skeleton) to core either the branches or  
168 any of the other types of lateral processes occurring in the body, depending on the genera and  
169 species. In addition to this main supportive skeleton, there are thousands of smaller (< 100  $\mu\text{m}$ ;  
170 microscleres) hook-like spicules, being either simple hooks (sigmata) or tooth-bearing hooks  
171 (chelae). These are scattered through the internal mesenchyme-like tissue and, more importantly,  
172 also at the external epithelia, where they project part of their hooking structure out of the body to  
173 capture small crustaceans that may contact the external sponge surface. Some of these sponge  
174 species have additional microscleric spicules to reinforce the skeleton, but very few carnivorous  
175 species - and in only the genera *Asbestopluma* (Family Cladorhizidae) , *Euchelipluma* (Family  
176 Guitarridae) and *Esperiopsis* (Family Esperiopsidae) - have been described having hypersilicified  
177 spicules (called desmas). Desmas are usually confined to the basal body region, probably to  
178 strengthen the area through which the sponge attaches to the substrate (Vacelet, 2007).

179           Because carnivorous sponges lack the aquiferous system that conventionally transports  
180 ambient seawater into the sponge body and because the isotope signal of their silica spicules has  
181 never been assessed before, it is compelling to examine whether silicon fractionation values in  
182 carnivorous sponges differ from those measured in the more conventional, filter-feeding sponges. As  
183 carnivorous sponges are typically constrained to bathyal habitats (Vacelet, 2007), their skeletons  
184 may turn into a good tool to infer traits of deep regional water masses. The recent collection of a  
185 new species of desma-bearing cladorhizid to be formally described in the genus *Asbestopluma*  
186 (Goodwin et al., in prep.) has provided an unparalleled opportunity to investigate  $\delta^{30}\text{Si}$  and  $\delta^{18}\text{O}$  of  
187 its silica spicules.

188

189 **Methods:**

190 *Specimen:*

191 Specimen DH19-2 (*Asbestopluma* sp.) was recovered by Hein Dredge from Burdwood Bank  
192 (1500-1530 m water depth, 54° 45'S, 62° 16'W) in the Atlantic Sector of the Southern Ocean from  
193 the R/V Nathaniel B. Palmer in 2011 (National Science Foundation NBP1103). The specimen was  
194 photographed and dried for transportation. Temperature, salinity, and Si(OH)<sub>4</sub> concentrations of the  
195 ambient water are estimated as 2.5-3°C, 34.5, and 60 μM, respectively (from on-board  
196 measurements and literature data available at [www.eWOCE.org](http://www.eWOCE.org)).

197 The specimen has an upright, moderately branching form (Figure 1). The basal body portion  
198 contains internally interlocked desmas (Figure 2A-B), externally surrounded by layer of microscleric  
199 acanthotylostrongyles (Figure 2B) and scarce sigmas. It is worth noting that the abundance of  
200 desmas decreases significantly from the basal body portion to the branch tips and that the  
201 acanthotylostrongyles occur exclusively at basal portion of the sponge. Further up the axis, the stem  
202 is cored by large smooth monoactines (styles), with smaller styles and diactines with rounded ends  
203 (anisostrongyles) outside this core, sigmas and chelae microscleres are also present (Figure 2C).  
204 Desmas become less frequent with increasing distance from the base (with desmas representing  
205 approximately 90% of the spicules from A, 50% from B, 40% from C and less than 25% from D and E)  
206 so that at the growth tips, there are only styles, sigma and chelae.

207

208 *Sample preparation:*

209 Five sponge tissue samples (A to E) were taken along the body length of the specimen, that  
210 is, at increasing distance from the attachment point, covering from the base to the branch tip (Figure  
211 1). Samples were cleaned for organic matter by heating to 80°C in 30% hydrogen peroxide for at  
212 least an hour and rinsing thoroughly in deionised water at least three times. At this stage, for each  
213 tissue sample, two skeletal subsamples were obtained from: 1) the spicules of the axial skeleton  
214 (axial or "internal" samples), and 2) the spicules of the radiating skeleton and the external  
215 epithelium (extra-axial or "external" samples). The subsamples were then heated to 80°C in trace  
216 metal grade concentrated nitric acid for at least an hour, and rinsed thoroughly in 18 MΩ.cm Milli-Q  
217 water at least three times. Standards and samples were prepared by alkaline fusion with sodium  
218 hydroxide pellets, acidified with ultra-clean nitric acid (Optima), and purified using cation exchange  
219 resin (Georg et al., 2006). Note that heating opal to 80°C during the organic matter removal process  
220 does not result in additional fractionation of spicule silicon isotopes (Hendry et al., 2011). Although  
221 there is no available information specifically about modern sponge spicules, heating samples of  
222 phytolith opal to 80°C during cleaning does not result in additional fractionation of oxygen isotopes



223 ~~Although there is no available information specifically about modern sponge spicules, heating~~  
224 ~~samples of opal to over 70°C during cleaning does not result in additional fractionation of oxygen~~  
225 ~~isotopes (Crespin et al., 2008). One study suggests that heating diatom opal to over 60°C results in a~~  
226 ~~potential offset in  $\delta^{18}\text{O}$  as a result of dissolution (Crespin et al., 2008). However, the  $\delta^{18}\text{O}$  values from~~  
227 ~~70 and 90°C from this study were within analytical error of the values of diatoms treated at 60°C.~~  
228 ~~Furthermore, heating of diatom opal to 70°C using different cleaning methods does not result in~~  
229 ~~measurable changes in  $\delta^{18}\text{O}$  (Tyler et al., 2007). (Tyler et al., 2007; Hendry et al., 2011), and~~  
230 ~~H~~heating to higher temperatures of 80-90°C is routine in downcore spicule opal  $\delta^{18}\text{O}$  analyses (e.g.  
231 Snelling et al., 2014).

232

### 233 *Silicon isotope analysis:*

234 The samples were analysed for silicon isotope ratios ( $^{29}\text{Si}/^{28}\text{Si}$ ,  $^{30}\text{Si}/^{28}\text{Si}$ ) using a Thermo  
235 Neptune Multi-Collector Inductively Coupled Plasma Mass Spectrometer (MC-ICP-MS) at Bristol  
236 University (Bristol Isotope Group). The isotope ratios were measured using 20 cycles per block.  
237 Machine blanks were monitored, and were <1% of the signal on  $^{28}\text{Si}$ . Mass bias and matrix effects  
238 were corrected using standard-sample bracketing, and internal Mg-doping (Cardinal et al., 2003;  
239 Hendry and Robinson, 2012). Silicon and magnesium intensities were matched within 10% (typically  
240 <5%). The results are reported as  $\delta^{30}\text{Si}$  values relative to the standard NBS28 (RM8546). Analysis of  
241 “diatomite” during the study yielded a mean  $\delta^{30}\text{Si}$  value of  $-1.25\text{‰}$  ( $\pm 0.18$  2SD,  $n = 70$ ); “big-batch”  
242 yielded a mean  $\delta^{30}\text{Si}$  value of  $-10.67\text{‰}$  ( $\pm 0.08$  2SD,  $n = 3$ ) (Reynolds et al., 2007). Repeat analyses of  
243 sponge standard LMG08 (Hendry and Robinson, 2012) during each run were used to assess long-  
244 term external reproducibility, and yielded a mean  $\delta^{30}\text{Si}$  value of  $-3.41\text{‰}$  over 6 months ( $\pm 0.16$  2SD,  
245  $n = 31$ ).  $\delta^{29}\text{Si}/\delta^{30}\text{Si}$  for all samples and standards was  $\sim 0.51$ , consistent with mass-dependent  
246 fractionation (Cardinal et al., 2003).

247

### 248 *Oxygen isotope analysis:*

249 Aliquots of spicule samples were analysed for oxygen isotope ratios ( $^{18}\text{O}/^{16}\text{O}$ ) following a  
250 step-wise fluorination procedure (Leng and Sloane, 2008) verified through an inter-laboratory  
251 calibration exercise (Chapligin et al., 2011). Samples were outgassed in nickel reaction vessels and  
252 reacted with  $\text{BrF}_5$  for 6 minutes at 250°C to remove all Si-OH bonds. Oxygen from Si-O-Si bonds was  
253 subsequently released by reaction with further reagent overnight at 550°C before being converted  
254 and collected as  $\text{CO}_2$ . Oxygen isotope measurements were made on a Finnigan MAT 253 with values  
255 converted to the VSMOW scale using the run laboratory diatom standard  $\text{BFC}_{\text{mod}}$  calibrated against  
256 NBS28. Repeat analysis of  $\text{BFC}_{\text{mod}}$  indicates reproducibility is 0.6‰ (2SD) (Leng and Sloane, 2008).

257

258 *Electron microscopy:*

259 Scanning electron microscopy (SEM) was used to describe the siliceous skeleton at the various body  
260 regions. An aliquot of spicules from each subsample was mounted onto an SEM aluminium stub,  
261 coated by gold sputtering and imaged using a HITACHI S-3500N Scanning Electron Microscope.  
262 To document the presence/absence of an axial canal at the core of the various spicules types, 1mm<sup>3</sup>  
263 sponge tissue samples were collected, placed onto a glass cover slip and subsequently cleaved  
264 multiple times to fracture the spicules using a scalpel blade under a dissecting scope. The cover slip  
265 with the cleaved tissue was placed onto a glass slide and, to eliminate the organic matter from the  
266 silica skeleton, three drops of concentrate nitric acid were added on the tissue sample while  
267 maintaining the slide above the flame of an alcohol burner. After boiling and evaporation of acid,  
268 new acid drops were added and the operation repeated several times until corroborating through a  
269 light microscope that the silica spicules were externally cleaned from organic remains, before rinsing  
270 three times in milli-Q water. The slip bearing the cleaned, fractured spicules mounted onto an SEM  
271 aluminium stub and coated by gold sputtering for further observation of fracture planes and axial  
272 canals using a HITACHI TM300 Scanning Electron Microscope.

273

274 **Results:**

275 *Silicon isotopes:*

276 The average  $\delta^{30}\text{Si}$  value for the cladorhizid DH19-2 was  $-0.37\text{‰}$ , but values ranged from  $-$   
277  $1.35$  to  $+0.59\text{‰}$ , with an overall range of  $1.94\text{‰}$  (Figure 3). These values fall within the total range  
278 of modern sponge  $\delta^{30}\text{Si}$  measurements in the literature (e.g. Hendry & Robinson, 2012). Since  
279 previous studies have found no discernible variation within an individual (Hendry et al., 2010;  
280 Hendry et al., 2011), this is an unprecedented variability within a single specimen, and represents  
281 approximately 40% of the total range of isotope values for existing calibrations ( $\sim 5\text{‰}$ ) (Hendry and  
282 Robinson, 2012). The external spicules were significantly and consistently isotopically lighter than  
283 the internal interlocking spicules. The external and internal spicules became isotopically heavier and  
284 lighter respectively along the axis, such that the difference between the internal and external  
285 spicules decreased away from the base of the specimen (from approximately  $1.4\text{‰}$  at A to  
286 approximately  $0.1\text{‰}$  at E; Figure 3).

287

288 *Oxygen isotopes:*

289 The average  $\delta^{18}\text{O}$  value for DH19-2 was  $+37.7\text{‰}$ , ~~but ranging~~ from  $+36.7$  to  $+38.7\text{‰}$   
290 (Figure 4), giving a range of  $2\text{‰}$ . The  $\delta^{18}\text{O}$  of the marine specimen in this study is significantly heavier

291 than values obtained for freshwater sponge spicules (approximately +22 to +30‰). ~~The, with~~  
292 ~~fractionation factors ( $\Delta\delta^{18}\text{O}_{\text{silica-seawater}}$ ) for the marine sponge (+36 to +39‰) was greater than that of~~  
293 ~~freshwater sponges of approximately (+28‰) and +36 to +39‰ for the fresh and saline water~~  
294 ~~sponges respectively~~ (Matteuzzo et al., 2013). The variation within the one individual from this study  
295 compares to an entire range of  $\delta^{18}\text{O}_{\text{water}}$  of less than 0.8‰ and potential temperature variations of  
296  $\sim 5^\circ\text{C}$  across the Drake Passage (Meredith et al., 1999), and represents nearly half of the 5‰  
297 variations found in a downcore sponge spicule  $\delta^{18}\text{O}$  record from Pliocene sediments (Snelling et al.,  
298 2014). The external spicules were consistently isotopically lighter than the internal interlocking  
299 spicules, although the difference between them (0.4 to 1‰) is approximately the same as the  
300 analytical error (2SD of 0.6‰). The trend in  $\delta^{18}\text{O}$  along the axis of the specimen is less clear than for  
301  $\delta^{30}\text{Si}$ : both the external and internal spicules because isotopically heavier from A to C, and then  
302 isotopically lighter from C to E. There is also a positive correlation between  $\delta^{30}\text{Si}$  and  $\delta^{18}\text{O}$  ( $r=0.88$ ,  
303  $p=0.001$ ,  $n=10$ ).

304

#### 305 **Discussion:**

##### 306 *Silicon isotopes and internal fractionation:*

307 The large variation in both isotope systems within the studied individual relates to a  
308 differential distribution of the spicule types along the sponge body (i.e., distance from sponge base),  
309 and also to differences in the abundance of given spicule types between the internal (axial) and  
310 external (extra-axial) body regions. The external basal skeleton (i.e., mostly acanthotylostrongyles)  
311 has the most isotopically light (negative)  $\delta^{30}\text{Si}$  that lies close to the existing  $\delta^{30}\text{Si}$ - $\text{Si}(\text{OH})_4$  calibration  
312 curve (Figure 5). The internal basal skeleton (i.e., mostly desmas) has a very isotopically heavy  
313 (positive)  $\delta^{30}\text{Si}$  compared to that of the external spicules, which may relate to the presence of desma  
314 spicules.

315 The desmas of this carnivorous sponge have an unusual formation mechanism compared to  
316 other megascleric demosponge spicules. Nearly all types of megascleric spicule, including most  
317 desmas, show an internal or "axial" canal (Fig. 6A). This canal originally harbours a filament of the  
318 enzymatic protein silicatein (Shimizu et al., 1998), responsible for initiating the polymerization of  
319 biogenic silica, the growth of which starts intracellularly through an enzymatically-guided  
320 polycondensation of dissolved silicon. The term "desmas" represents a large variety of  
321 phylogenetically unrelated spicule morphologies, which only share the feature of being massive,  
322 relatively irregular skeletal pieces produced by hypersilicification, and may or may not possess an  
323 axial canal. How and where the hypersilicification of desmas is achieved remains poorly understood.  
324 In all cases described to date, the desmas in carnivorous sponges are anaxial, that is, lack axial canals

325 (Figure 6B). The absence of an axial canal indicates that their silicification does not involve an initial  
326 intracellular, enzyme-guide silica polymerization. Consequently, these anaxial desmas must grow via  
327 a mechanism different from that taking place in other demosponge spicules, which may account for  
328 their distinctive silicon and oxygen isotopic composition. This idea is in agreement with previous  
329 findings indicating that some cellular mechanisms for spicule silicification may have evolved  
330 independently in different sponge lineages (Maldonado and Riesgo, 2007). The level at which the  
331 secondary hypersilicification step of desmas could also contribute, if any, to their isotope signal  
332 remains unknown, and further study into the potential differences in the isotopic signal between  
333 desmas with and without axial canals is required.

334           The decreasing abundance of desmas with increasing distance from the sponge base is at  
335 least one of the plausible factors responsible for the within-sponge variation in isotope compositions  
336 observed in this study. We suggest that the likely extracellular silicification of these desmas could  
337 result in kinetic fractionation of silicon isotopes. It should also be noted that the external basal  
338 spicules (i.e., the acanthotylostrongyles), although forming the “best fit” to the existing  $\delta^{30}\text{Si-Si(OH)}_4$   
339 calibration, are still outside of analytical error of the calibration curve, and this offset could be  
340 explained by some desma contamination (Figure 2b).

341           Further up the axis away from the base, the extra-axial styles have a higher  $\delta^{30}\text{Si}$ , moving  
342 further away from the existing  $\delta^{30}\text{Si-Si(OH)}_4$  calibration curve (Figure 5), and then lower again  
343 towards the growing tip. This does not reflect contamination from microscleres (i.e., sigmas and  
344 chelae), as individually picked and cleaned styles are within analytical uncertainty ( $\pm 0.15\%$ ) of the  
345 bulk measurement (see white box on Figure 3). Although the internal styles also become isotopically  
346 enriched, the difference between the internal and external spicule  $\delta^{30}\text{Si}$  declines up the axis, most  
347 likely because of a decline in the number of desmas.

348           There are also two alternative, but probably less plausible explanations, for the large intra-  
349 individual silicon isotopic variation along the body axis. One is that this sponge grows extremely slowly  
350 (over centuries) in the deep-sea environment. If so, it could be that during the first decades of its life,  
351 what is now the basal body portion was exposed to a water mass with temperature and silicic acid  
352 concentration different from present, progressively changing overtime towards the current values and  
353 impacting accordingly the isotope signal during sponge growth. A second possibility is that this sponge  
354 grows very rapidly. If so, the basal portion could have been formed during an episodic input of  
355 seawater with abnormal silicic acid concentration and temperature, compared to the ambient  
356 conditions during the subsequent growth. Because virtually nothing is known about the longevity and  
357 growth rate of these sponges, these ideas remain mere speculation.

358            Could the heavy silicon isotope bias be a consequence of the absence of an aquiferous system  
359 in the carnivorous sponge? Given that the aquiferous system usually allows the circulation of ambient  
360 seawater throughout the body, the loss of this system could result in internal silicon isotope  
361 fractionation as the isotopes in the aqueous component becomes progressively heavier due to  
362 precipitation of silica in a closed system. This process would explain not only the offset between the  
363 external and internal spicules but also the trends along the length of the sponge stem. Again, nothing  
364 is known about how the dissolved silicon molecules are transported into the body by these sponges  
365 or about the average replenishment rate for dissolved silicon within the internal tissues. Nevertheless,  
366 if a simplified silicon isotope fractionation model is formulated, ignoring the impact of desmas and  
367 assuming a variable silicon isotopic fractionation during sponge growth according to the core top  
368 spicule calibration of Hendry and Robinson (2012), we can examine the impact of an isotopically closed  
369 system on changes in spicule composition with cellular silicon utilisation (Figure 7). This simplified  
370 model suggests that relatively small degrees of cellular silicon utilisation (less than 30%) could result  
371 in heavier  $\delta^{30}\text{Si}$  observed up the axis of the *Asbestopluma sp.* specimen. A higher rate of dissolved  
372 silicon replenishment and a faster sponge growth rate could explain the return to lighter isotopic  
373 compositions at the growing tips.

374

375 *Oxygen isotopes and additional fractionation processes:*

376            The positive correlation that we find within one individual between  $\delta^{30}\text{Si}$  and  $\delta^{18}\text{O}$  indicates  
377 that there may be some shared mechanisms behind fractionation of the two isotope systems, at least  
378 in *Asbestopluma*. There is a similar systematic offset between the external and internal spicules in  
379  $\delta^{18}\text{O}$  as for  $\delta^{30}\text{Si}$  values, suggesting that the unusual silicification process that results in desma  
380 formation may fractionate oxygen isotopes in a similar manner to silicon. However, the along-axis  
381 trend is less clear in the  $\delta^{18}\text{O}$  than  $\delta^{30}\text{Si}$ , suggesting desmas cause a smaller bias in oxygen isotope  
382 systematics than for silicon. Furthermore, there is no significant along-axis decrease in  $\delta^{18}\text{O}$  in the  
383 internal spicules, as observed for  $\delta^{30}\text{Si}$ , suggesting that any internal fractionation of oxygen isotopes  
384 is less pronounced and within the analytical uncertainty.

385            Additional processes active at the surface of the sponge spicule silica may also have an  
386 influence on both the silicon and oxygen isotope values, including precipitation processes and  
387 dissolution. There is some evidence from one laboratory study for a silicon isotope fractionation  
388 during dissolution of diatom opal (Demarest et al., 2009), which is not supported by more recent  
389 laboratory and field studies (Egan et al., 2012; Wetzel et al., 2014). Although there is potential for  
390 kinetic fractionation of oxygen during dissolution and reprecipitation of silica (Crespin et al., 2008;  
391 Dodd et al., 2012), further work is required to investigate whether ~~There is no available information~~

392 ~~en~~ fractionation of either silicon or oxygen isotopes occurs during the dissolution of sponge spicules,  
393 or by any additional surface precipitation processes.

394

#### 395 **Implications for palaeoclimate and outlook:**

396 This first study of within-sponge differential fractionation has a number of implications for  
397 biomineralisation and the use of isotope proxies for reconstructing past nutrient conditions. Firstly,  
398 our findings suggest that internal non-equilibrium fractionation of silicon isotopes in sponges can  
399 occur, depending on silicic acid replenishment rates in the internal tissues, which could explain some  
400 of the scatter in the  $\delta^{30}\text{Si}$ - $\text{Si}(\text{OH})_4$  calibration plot (Hendry and Robinson, 2012). Internal fractionation  
401 could also impact sponge  $\delta^{18}\text{O}$ , but less severely. We suggest that the anaxial desmas of this and  
402 probably other carnivorous sponges have a different mode of silicification causing an unusual  
403 isotopic signature in their biogenic silica.

404 Secondly, this study highlights the need for caution when preparing samples in order to compile  
405 robust palaeoclimate archives. A large number of spicules should be picked for such archives in  
406 order to “average” out variations caused by kinetic fractionation in Cladorhizid sponges, which  
407 cannot be readily distinguished using light microscopy. Furthermore, desma formation may result in  
408 very different fractionation behaviour. However, desmas are morphologically distinct, and should be  
409 excluded from proxy measurements for palaeoclimate applications until further studies have been  
410 completed to assess the level at which these spicules result in isotopic bias. Whether axial and  
411 anaxial desmas can provide an independent complementary proxy to corroborated trends inferred  
412 from the "conventional" silica spicules is a possibility that needs to be explored in future studies.

413

#### 414 **Author contributions:**

415 KRH and GS/HS/ML carried out the isotope and SEM analyses, and CG/JB carried out the sponge  
416 identification, MM carried out further SEM and spicule analyses. All authors contributed  
417 significantly to discussions and the preparation of the manuscript.

418

#### 419 **Acknowledgements:**

420 The authors would like to thank C. Coath (Bristol) for assistance with mass spectrometry, L.  
421 Robinson (Bristol), R. Waller (Maine), the captain and crew of the R/V Nathaniel B. Palmer. Samples  
422 were processed in the laboratories at Cardiff University, with thanks to R. Perkins. SEM images were  
423 taken at the University of Bristol with the assistance of S. Kearns, B. Buse and A. Anton-Stephens,  
424 and at CEAB-CSIC, Blanes. This work was funded by the National Science Foundation (grants  
425 0944474, 0636787 and 1029986), The Leverhulme Trust (Research Grant RPG-2012-615); KH is

426 funded by the Royal Society. MM is funded by the Spanish Ministry of Innovation and  
427 Competitiveness (CTM2012-37787). CG is a research associate at Queen's University Marine  
428 Laboratory, Portaferry. The authors would like to thank two anonymous reviewers for their  
429 constructive comments.  
430

431 **Figure captions:**

432 Figure 1: Specimen DH19-2, *Asbestopluma* sp. Scale bar shows 1 cm. Red boxes show subsampling  
433 sections A-E.

434 Figure 2: Scanning electron microscope images of subsamples from DH19-2 *Asbestopluma* sp. A)  
435 Internal framework section A, near the base; B) External section A, near the base; C) Internal section  
436 E, the growing tip Abbreviations: des = desma, ani = anisostrongyles, aca = acanthotylostrongyles, sty  
437 = styles.

438 Figure 3:  $\delta^{30}\text{Si}$  values for subsamples of DH19-2. Red bars show the internal interlocking framework,  
439 black bars show the external loose spicules, and green bars show the difference between the  
440 internal and external spicules. Hollow rectangular symbol shows the isotopic composition of  
441 individually picked and cleaned styles from the growing tip. Error bars show external reproducibility  
442 from replicate standard measurements (2SD).

443 Figure 4:  $\delta^{18}\text{O}$  values for subsamples of DH19-2. Red bars show the internal interlocking framework,  
444 black bars show the external loose spicules, and green bars show the difference between the  
445 internal and external spicules. Error bars show external reproducibility from replicate standard  
446 measurements (2SD).

447 Figure 5: Comparison of  $\delta^{30}\text{Si}$  and  $\Delta\delta^{30}\text{Si}$  ( $= \delta^{30}\text{Si}_{\text{sponge}} - \delta^{30}\text{Si}_{\text{seawater}}$ ) results from DH19-2 *Asbestopluma*  
448 sp. (red symbols) and existing calibration (black symbols). Data for sponge  $\delta^{30}\text{Si}$  and references for  
449 seawater  $\delta^{30}\text{Si}$  from (Hendry et al., 2010; Hendry and Robinson, 2012; Wille et al., 2010).

450 Figure 6: Scanning electron microscope images of fracture plane of *Asbestopluma* sp. spicules. (A-B)  
451 Megascleric styles showing the internal axial canal (ac) (scale bar 30  $\mu\text{m}$ ). (C-D) Core area (co) of  
452 anaxial desmas of the cladorhizid DH19-2 showing the absence of axial canal (scale bar 20  $\mu\text{m}$ ).

453 Figure 7: Sponge fractionation model for internal Si in an isotopically closed system. We assume a  
454 variable fractionation factor  $\epsilon'$  that approximates  $\Delta\delta^{30}\text{Si}$  from the core top spicule calibration curve  
455 of Hendry & Robinson (2012):

456 
$$\Delta\delta^{30}\text{Si} = -6.54 + (270/(53+[\text{Si}(\text{OH})_4])$$

457 The internal dissolved Si will fractionate according to:

458 
$$\delta^{30}\text{Si}(\text{OH})_{4\text{internal}} = \delta^{30}\text{Si}(\text{OH})_{4\text{initial}} + \epsilon' * \ln(f)$$

459 Where f is the fraction of dissolved Si left available internally. The  $\delta^{30}\text{Si}$  of the spicules that form  
460 from this Si depleted fluid is then given by:

461 
$$\delta^{30}\text{Si} = \delta^{30}\text{Si}(\text{OH})_{4\text{internal}} + \epsilon'$$

462

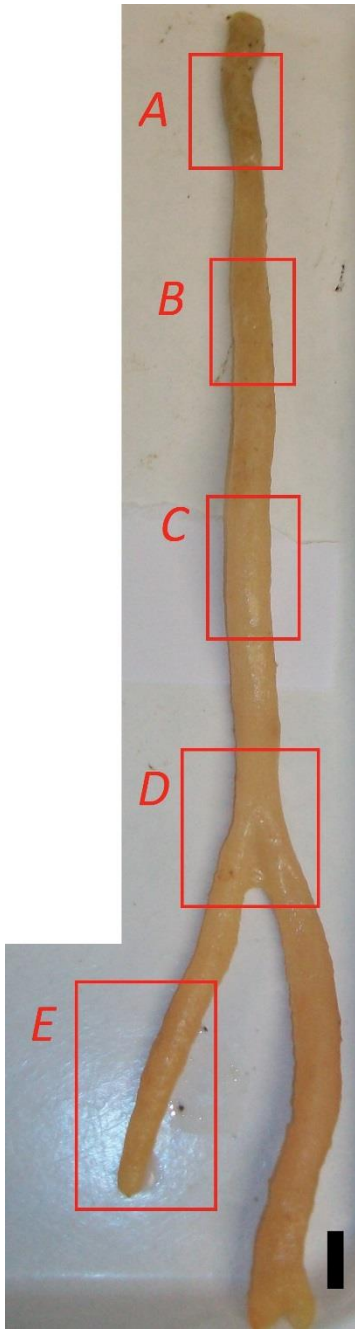


463 Table 1: Stable isotope results for DH19-2 *Asbestopluma* sp. specimen

Subsample	Internal		External	
	$\delta^{30}\text{Si}$ (‰)	$\delta^{18}\text{O}$ (‰)	$\delta^{30}\text{Si}$ (‰)	$\delta^{18}\text{O}$ (‰)
A	+0.02	+37.74	-1.35	+36.71
B	+0.59	+38.40	-0.84	+37.68
C	+0.48	+38.69	-0.59	+38.02
D	+0.05	+37.98	-0.53	+37.54
E	-0.68	+37.61	-0.86	+36.96

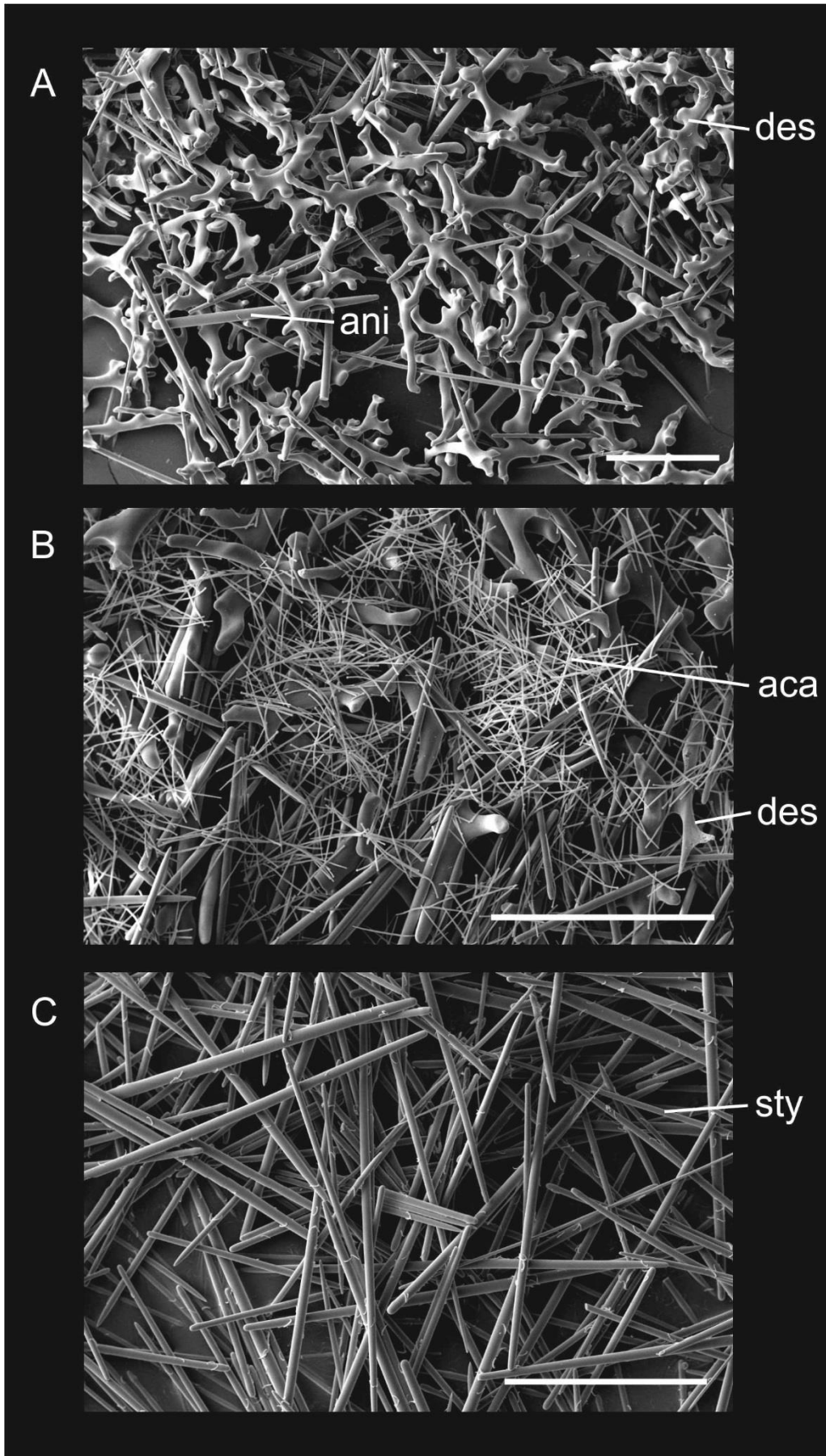
464





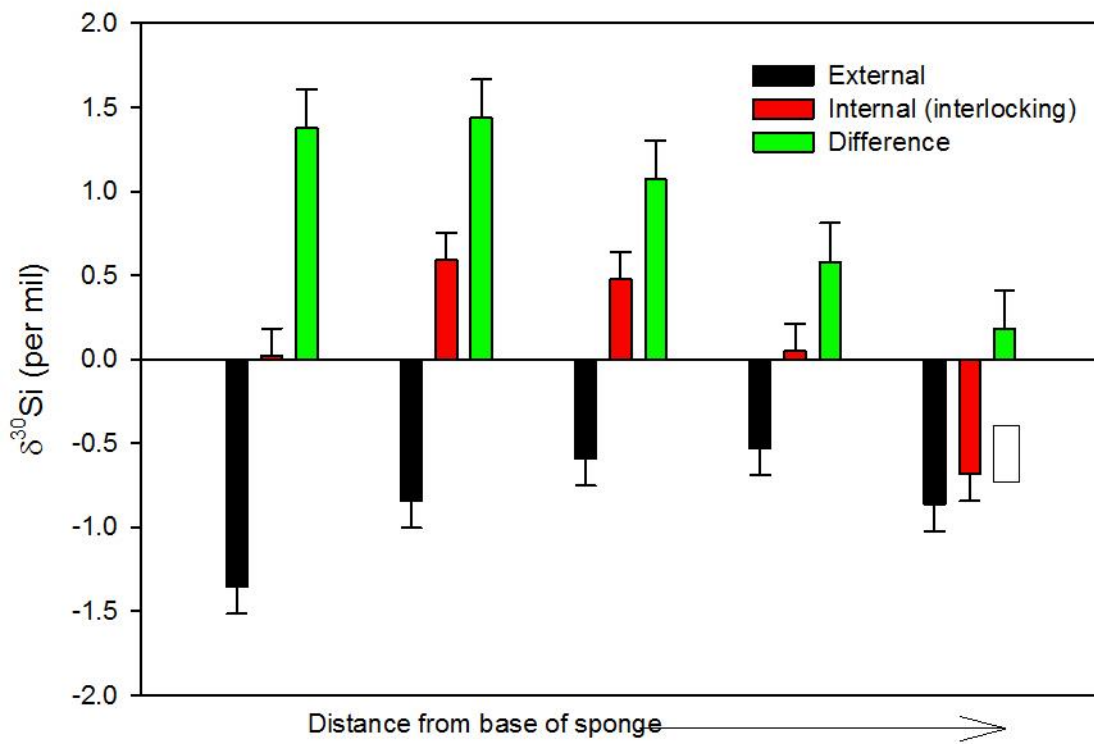
466  
467

Figure 1



468  
469

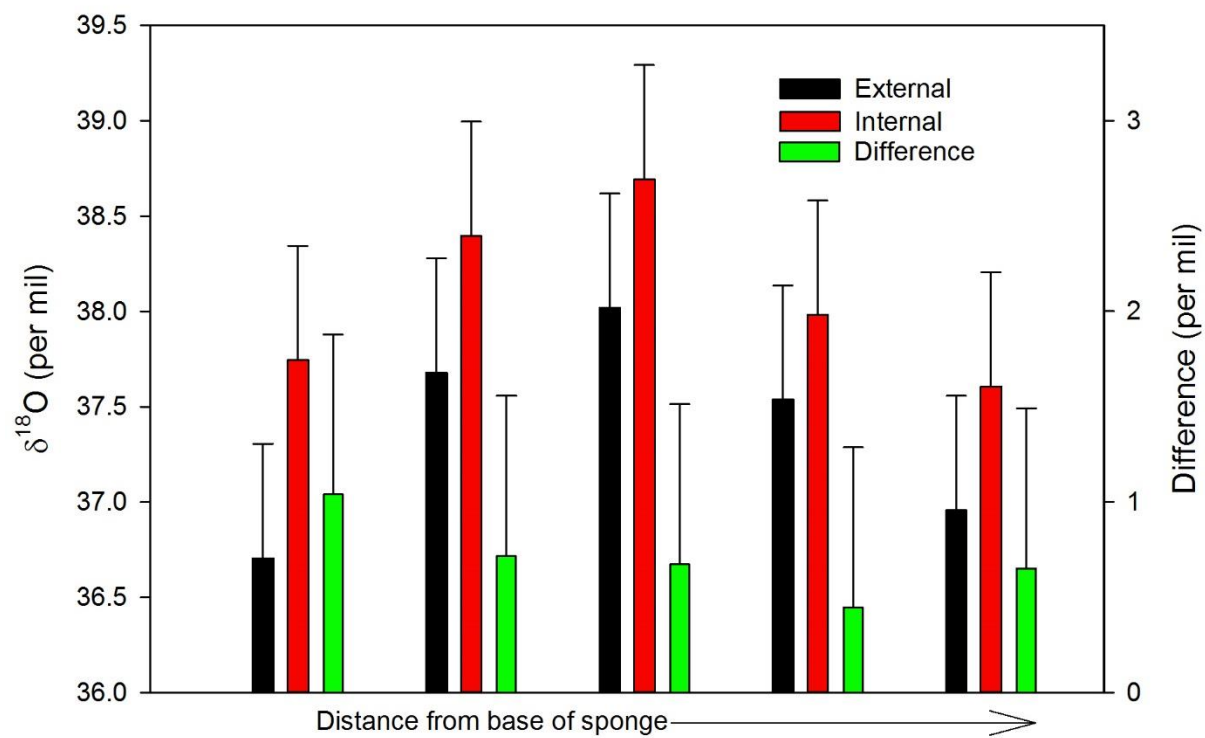
Figure 2



470

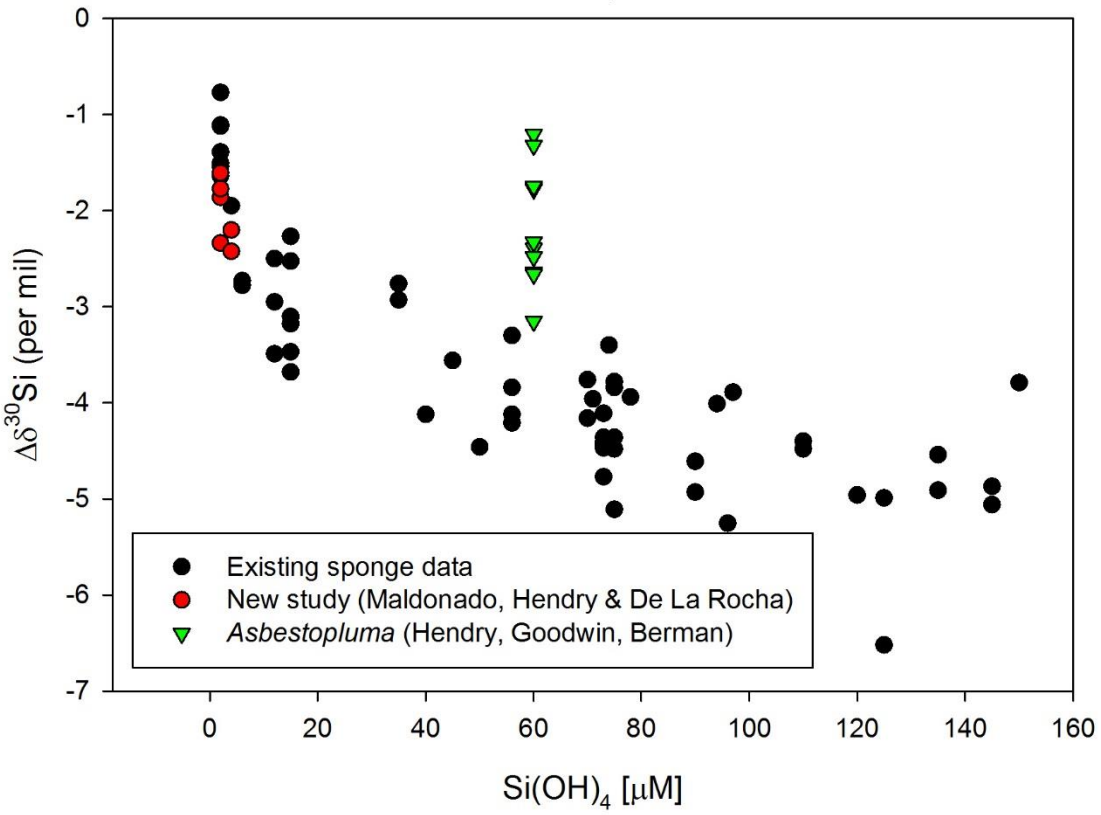
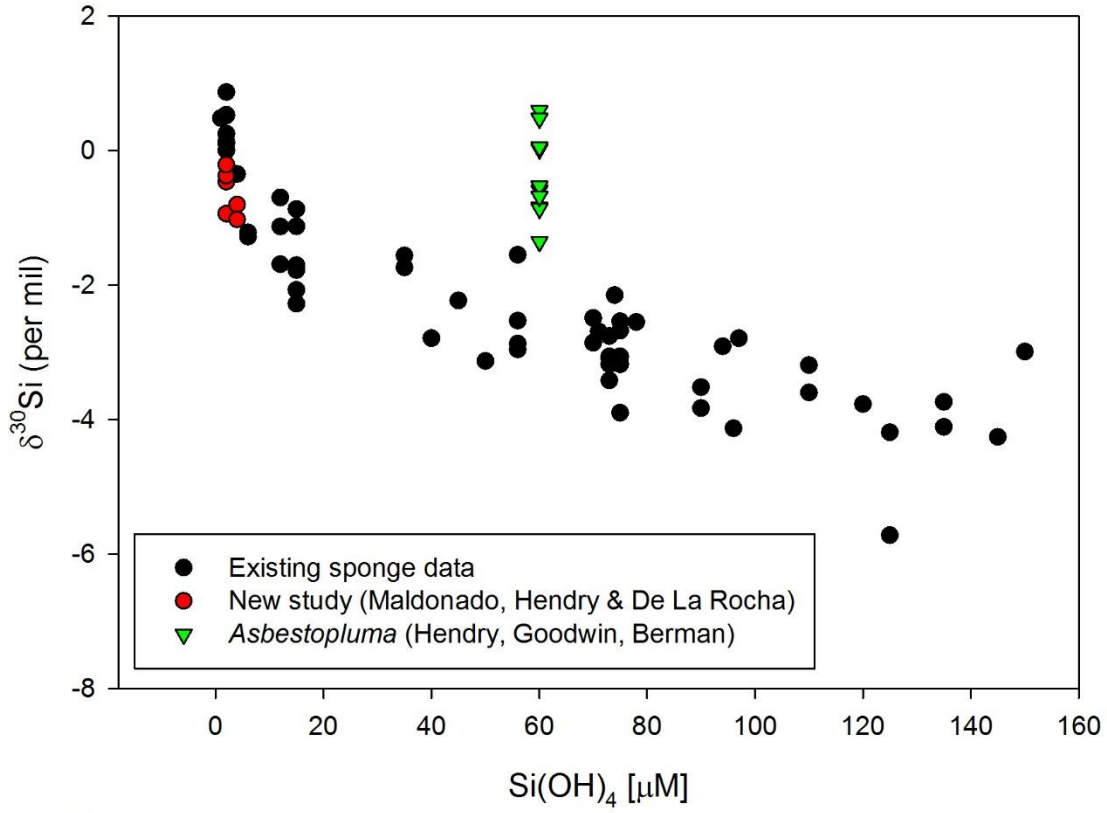
471 Figure 3

472



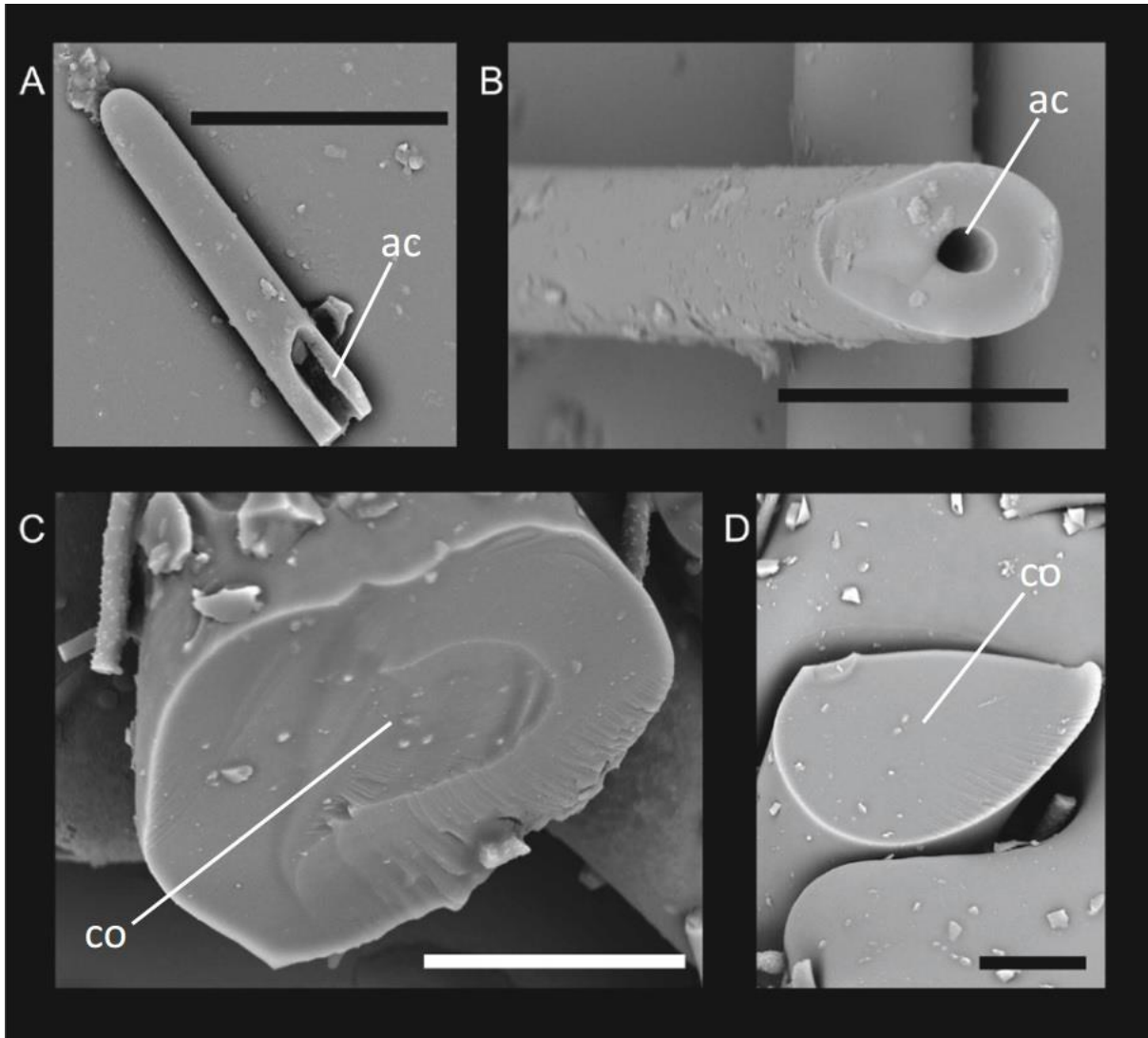
474

475 Figure 4



476

477 Figure 5

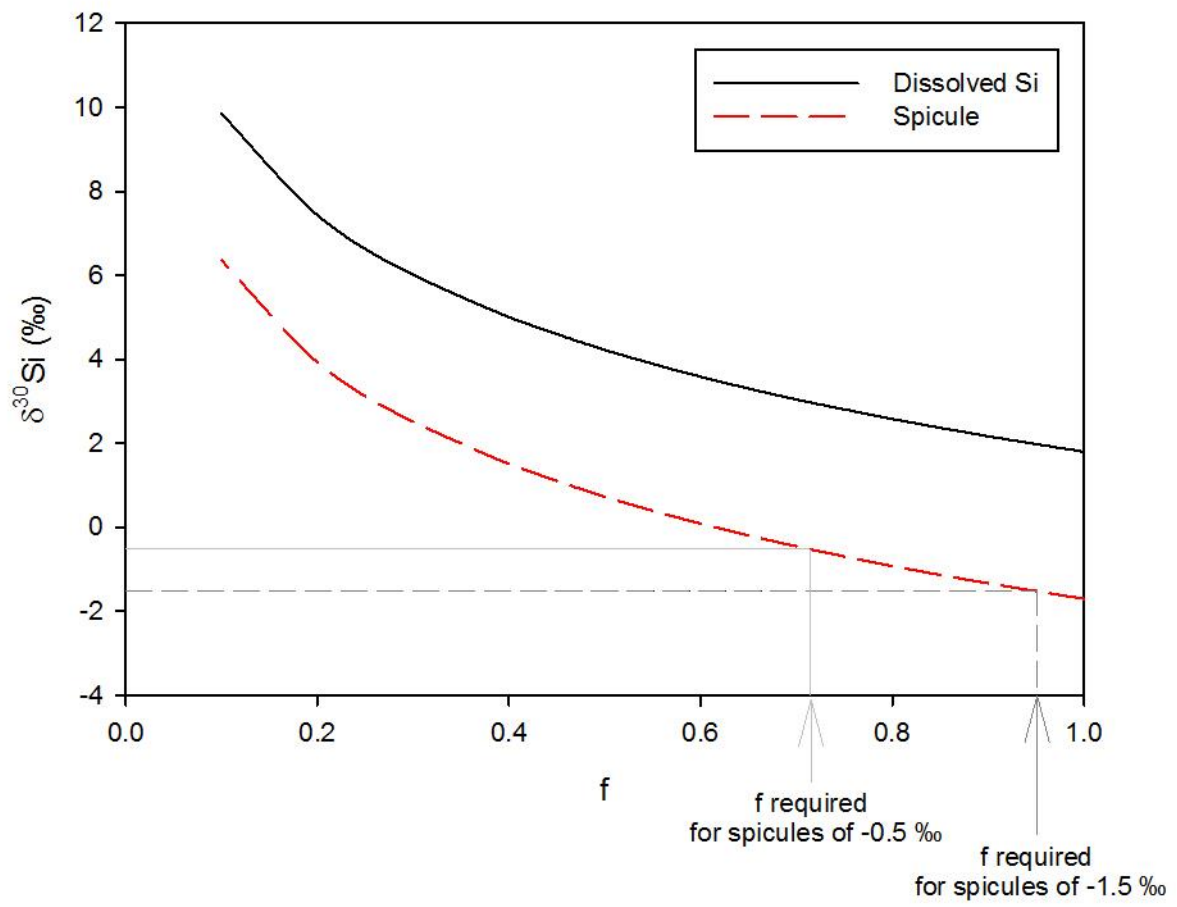


478

479

Figure 6





480

481 Figure 7

482 **References:**

483

484 Aguilar, R., Correa, M. L., Calcinai, B., Pastor, X., & De la Torriente, A. First records of *Asbestopluma*  
485 *hypogea* Vacelet and Boury-Esnault, 1996 (Porifera, Demospongiae Cladorhizidae) on  
486 seamounts and in bathyal settings of the Mediterranean Sea. *Zootaxa*, 2925, 33-40, 2011.

487 Bakran-Petricioli, T., Vacelet, J., Zibrowius, H., Petricioli, D., and Chevaldonné, P. New data on the  
488 distribution of the 'deep-sea' sponges *Asbestopluma hypogea* and *Oopsacas minuta* in the  
489 Mediterranean Sea. *Marine Ecology*, 28(s1), 10-23, 2007.

490 Cardinal, D., Alleman, L. Y., de Jong, J., Ziegler, K., and Andre, L. Isotopic composition of silicon  
491 measured by multicollector plasma source mass spectrometry in dry plasma mode. *Journal*  
492 *of Analytical Atomic Spectrometry*, 18, 213-218, 2003.

493 Chaplign, B., Leng, M. J., Webb, E., Alexandre, A., Dodd, J. P., Ijiri, A., Lücke, A., Shemesh, A.,  
494 Abelmann, A. and Herzschuh, U. Inter-laboratory comparison of oxygen isotope  
495 compositions from biogenic silica. *Geochimica et Cosmochimica Acta*, 75(22), 7242-7256,  
496 2011.

497 Chevaldonné, P., Pérez, T., Crouzet, J. M., Bay-Nouailhat, W., Bay-Nouailhat, A., Fourt, M., Almòn, b.,  
498 Pérez, J., Aguilar, R., and Vacelet, J. Unexpected records of 'deep-sea' carnivorous sponges  
499 *Asbestopluma hypogea* in the shallow NE Atlantic shed light on new conservation issues.  
500 *Marine Ecology*, doi:10.1111/maec.12155, 2014.

501 [Crespin, J., Alexandre, A., Sylvestre, F., Sonzogni, C., Pailles, C., and Garreta, V. IR laser extraction](#)  
502 [technique applied to oxygen isotope analysis of small biogenic silica samples, \*Analytical\*](#)  
503 [\*Chemistry\*, 80\(7\), 2372-2378, 2008.](#)

504 Demarest, M. S., Brzezinski, M. A. and Beucher, C. Fractionation of silicon isotopes during biogenic  
505 silica dissolution, *Geochimica et Cosmochimica Acta*, 73, 5572-5583, 2009.

506 [Dodd, J. P., and Sharp, Z.D. A laser fluorination method for oxygen isotope analysis of biogenic silica](#)  
507 [and a new oxygen isotope calibration of modern diatoms in freshwater environments,](#)  
508 [\*Geochimica et Cosmochimica Acta\*, 74\(4\), 1381-1390, 2010.](#)

509 Egan, K., Rickaby, R. E. M., Leng, M. J., Hendry, K. R., Hermoso, M., Sloane, H. J., Bostock, H. and  
510 Halliday, A.N. Diatom silicon isotopes as a proxy for silicic acid utilisation: A Southern Ocean  
511 core top calibration, *Geochimica et Cosmochimica Acta*, 96, 174-192, 2012.

512 Ellwood, M. J., Wille, M., and Maher, W. Glacial silicic acid concentrations in the Southern Ocean.  
513 *Science*, 330, 1088-1091, 2010.

514 Georg, R. B., Reynolds, B. C., Frank, M., and Halliday, A. N. New sample preparation techniques for  
515 the determination of Si isotopic composition using MC-ICPMS. *Chemical Geology*, 235, 95-  
516 104, 2006.

517 Hendry, K. R., Georg, R. B., Rickaby, R. E. M., Robinson, L. F., and Halliday, A. N. Deep ocean nutrients  
518 during the Last Glacial Maximum deduced from sponge silicon isotopic compositions. *Earth*  
519 *and Planetary Science Letters*, 292, 290-300, 2010.

520 Hendry, K. R., Leng, M. J., Robinson, L. F., Sloane, H. J., Blusztjan, J., Rickaby, R. E. M., Georg, R.B.,  
521 and Halliday, A.N. Silicon isotopes in Antarctic sponges: an interlaboratory comparison.  
522 *Antarctic Science*, 23, 34-42, 2011.

523 Hendry, K. R., and Robinson, L. F. The relationship between silicon isotope fractionation in sponges  
524 and silicic acid concentration: modern and core-top studies of biogenic opal. *Geochimica et*  
525 *Cosmochimica Acta*, 81, 1-12, 2012.

526 Hendry, K. R., Robinson, L. F., McManus, J. F., and Hays, J. D. Silicon isotopes indicate enhanced  
527 carbon export efficiency in the North Atlantic during deglaciation. *Nature Communications*,  
528 5., 05399, doi:10.1038/ncomms4107, 2014.

529 Hendry, K. R., and Brzezinski, M.A. Using silicon isotopes to understand the role of the Southern  
530 Ocean in modern and ancient biogeochemistry and climate. *Quaternary Science Reviews*, 89,  
531 13-26, 2014.

- 532 Leng, M. J., and Sloane, H. J. Combined oxygen and silicon isotope analysis of biogenic silica. *Journal*  
533 *of Quaternary Science*, 23, 313-319, 2008.
- 534 Leng, M. J., Swann, G. E. A., Hodson, M. J., Tyler, J. J., Patwardhan, S. V., and Sloane, H. J. The  
535 potential use of silicon isotope composition of biogenic silica as a proxy for environmental  
536 change. *SILICON*, 1, 65-77, 2009.
- 537 Lopes, D. A., Bravo, A., and Hajdu, E. New carnivorous sponges (Cladorhizidae: Poecilosclerida:  
538 Demospongiae) from off Diego Ramírez Archipelago (south Chile), with comments on  
539 taxonomy and biogeography of the family. *Invertebrate Systematics*, 25(5), 407-443, 2012.
- 540 Maldonado, M., Carmona, M. C., Uriz, M. J., and Cruzado, A. Decline in Mesozoic reef-building  
541 sponges explained by silicon limitation. *Nature*, 401, 785-788, 1999.
- 542 Maldonado, M., Carmona, M. C., Velásquez, Z., Puig, A., Cruzado, A., López, A., and Young, C. M.:  
543 Siliceous sponges as a silicon sink: An overlooked aspect of the benthopelagic coupling in the  
544 marine silicon cycle, *Limnol. Oceanogr.*, 50, 799-809, 2005.
- 545 Maldonado, M., Hooper, J. N. A., and Van Soest, R. W. M.: Family Pachastrellidae Carter, 1875. In:  
546 *Systema Porifera: A guide to the classification of sponges*, Kluwer Academic/Plenun Publisher,  
547 New York, 141-162, 2002.
- 548 Maldonado, M., Ribes, M., and Van Duyl, F. C.: Nutrient fluxes through sponges: biology, budgets, an  
549 ecological implications, *Adv. Mar. Biol.*, 62, 114-182, 2012.
- 550 Maldonado, M. and Riesgo, A.: Intra-epithelial spicules in a homosclerophorid sponge, *Cell Tissue*  
551 *Research*, 328, 639-650, 2007.
- 552 Matteuzzo, M., Alexandre, A., Varajão, A., Volkmer-Ribeiro, C., Almeida, A., Varajão, C., Vallet-  
553 Coulomb, C., Sonzogni, C., and Miche, H. Assessing the relationship between the  $\delta$  18 O  
554 signatures of siliceous sponge spicules and water in a tropical lacustrine environment (Minas  
555 Gerais, Brazil). *Biogeosciences Discussions*, 10(8), 12887-12918, 2013.
- 556 Meredith, M. P., Grose, K. E., McDonagh, E. L., Heywood, K. J., Frew, R. D., and Dennis, P. F.  
557 Distribution of oxygen isotopes in the water masses of Drake Passage and the South Atlantic.  
558 *Journal of Geophysical Research*, 104, 20949-20962, 1999.
- 559 Pike, J., Swann, G. E. A., Leng, M. J., and Snelling, A. M. Glacial discharge along the west Antarctic  
560 Peninsula during the Holocene. *Nature Geoscience*, 6, 199-202, 2013.
- 561 Pisera, A. Some aspects of silica deposition in lithistid demosponge desmas. *Microscopy research and*  
562 *technique*, 62(4), 312-326, 2003.
- 563 Reynolds, B. C., Aggarwal, J., Andre, L., Baxter, D., Beucher, C., Brzezinski, M. A., Engstrom, E., Georg,  
564 R.B., Land, M., Leng, M.J., Opfergelt, S., Rodushkin, I., Sloane, H.J., van der Boorn, S.H.J.M.,  
565 Vroon, P.Z., and Cardinal, D. An inter-laboratory comparison of Si isotope reference  
566 materials. *Journal of Analytical Atomic Spectrometry*, 22, 561-568, 2007.
- 567 Shimizu, K., Cha, J. N., Stucky, G. D., and Morse, D. E.: Silicatein alpha: cathepsin L-like protein in  
568 sponge biosilica, *Proc. Natl. Acad. Sci. USA*, 95, 6234-6238, 1998.
- 569 Van Soest, R.W.M; Boury-Esnault, N.; Hooper, J.N.A.; Rützler, K.; de Voogd, N.J.; Alvarez de Glasby,  
570 B.; Hajdu, E.; Pisera, A.B.; Manconi, R.; Schoenberg, C.; Janussen, D.; Tabachnick, K.R.,  
571 Klautau, M.; Picton, B.; Kelly, M.; Vacelet, J.; Dohrmann, M.; and Cristina Díaz, M.; Cárdenas,  
572 P. World Porifera database. Accessed at <http://www.marinespecies.org/porifera> on 2014-  
573 09-16, 2014.
- 574 Snelling, A. M., Swann, G. E. A., Pike, J., and Leng, M. J. Pliocene diatom and sponge spicule oxygen  
575 isotope ratios from the Bering Sea: isotopic offsets and future directions. *Clim. Past Discuss.*,  
576 10(3), 2087-2104, 2014.
- 577 Tréguer, P., and De la Rocha, C.L., The world ocean silica cycle, *Annual Review of Marine Science*, 5,  
578 477-501, 2013.
- 579 Tyler, J. J., Leng, M.J. and Sloane, H.J. The effects of organic removal treatment on the integrity of  
580  $\delta^{18}\text{O}$  measurements from biogenic silica, *Journal of Paleolimnology*, 37(4), 491-497, 2007.

581 Uriz, M. J., Turon, X., Becerro, M. A., and Agell, G. Siliceous spicules and skeleton frameworks in  
582 sponges: origin, diversity, ultrastructural patterns, and biological functions. *Microscopy*  
583 *Research and Technique*, 62, 279-299, 2003.

584 Vacelet, J. New carnivorous sponges (Porifera, Poecilosclerida) collected from manned submersibles  
585 in the deep Pacific. *Zoological Journal of the Linnean Society*, 148(4), 553-584, 2006.

586 Vacelet, J. Diversity and evolution of deep-sea carnivorous sponges. In: *Porifera research:*  
587 *biodiversity, innovation and sustainability* (Custódio, M.R.; Lôbo-Hadju. G., Hadju, E., Muricy,  
588 G eds) pp 107-115. Museu Nacional, Rio de Janeiro, 2007.

589 Vacelet, J., and Duport, E. Prey capture and digestion in the carnivorous sponge *Asbestopluma*  
590 *hypogea* (Porifera: Demospongiae). *Zoomorphology*, 123(4), 179-190, 2004.

591 Wetzel, F., de Souza, G., and Reynolds, B. What controls silicon isotope fractionation during  
592 dissolution of diatom opal?, *Geochimica et Cosmochimica Acta*, 131, 128-137, 2014.

593 Wille, M., Sutton, J., Ellwood, M. J., Sambridge, M., Maher, W., Eggins, S., and Kelly, M. Silicon  
594 isotopic fractionation in marine sponges: a new model for understanding silicon isotopic  
595 fractionation in sponges. *Earth and Planetary Science Letters*, 292, 281-289,  
596 doi:10.1016/j.epsl.2010.1001.1036, 2010.

597